FRACTURE TOUGHNESS AS A FUNCTION OF THE MODE MIXITY USING NON-CONVENTIONAL TECHNIQUES

Filipe J.P.Chaves

IDMEC- Pólo FEUP

L.F.M. da Silva

M.F.S.F. de Moura

DEMec - FEUP

D. Dillard

ESM – Virginia Tech

outline

Bonded joints in service are usually subjected to mixed-mode conditions due to geometric and loading complexities.

Consequently, the fracture characterization of bonded joints under mixed-mode loading is a fundamental task.

There are some conventional tests proposed in the literature concerning this subject, as is the case of the asymmetric double cantilever beam (ADCB), the single leg bending (SLB) and the cracked lap shear (CLS).

Nevertheless, these tests are limited in which concerns the variation of the mode-mixity, which means that different tests are necessary to cover the fracture envelope in the G_I-G_{II} space.

This work consists on the analysis of the different mixed mode tests already in use, allowing to design an optimized test protocol to obtain the fracture envelope for an adhesive, using a Double Cantilever Beam (DCB) specimen and a Compliance Based Beam Method (CBBM) for the data reduction scheme.

motivation

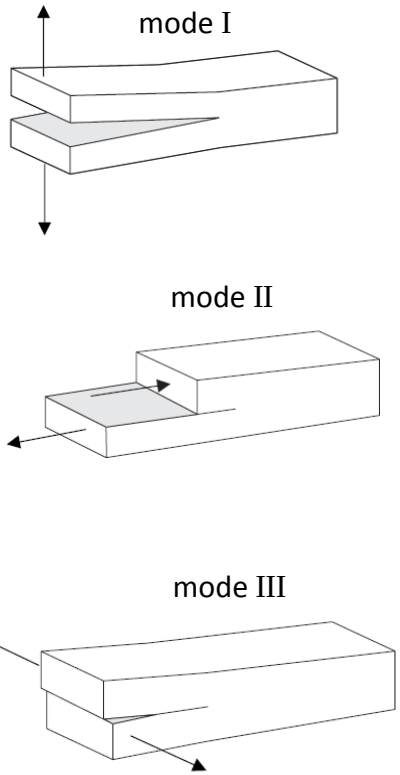

Figure 1. Fracture modes.

Mode I – opening mode (a tensile stress normal to the plane of the crack);

Mode II – Sliding mode (a shear stress acting parallel to the plane of the crack and perpendicular to the crack front);

Mode III – tearing mode (a shear stress acting parallel to the plane of the crack and parallel to the crack front)

fracture modes

Mode I release rate energy G_I is well known and well characterized.

DCB – Double Cantilever Beam

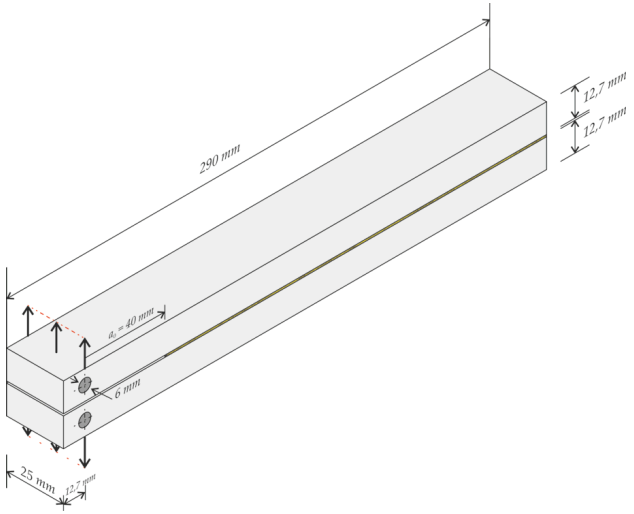

Figure2. DCB specimen and test.

&

ASTM D 3433 - 99

TDCB – Tapered Double Cantilever Beam

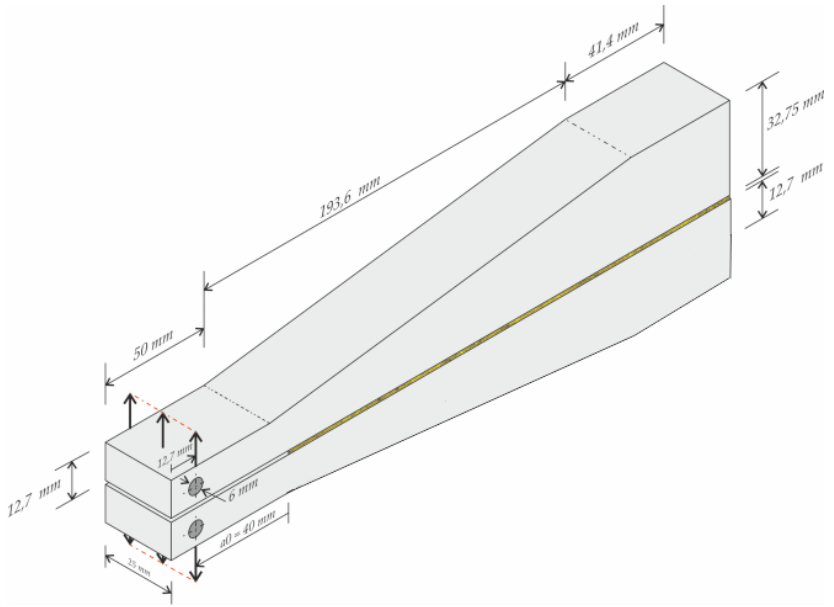

Figure 3. TDCB specimen and test.

fracture tests [mode I]

ENF – End Notch Flexure

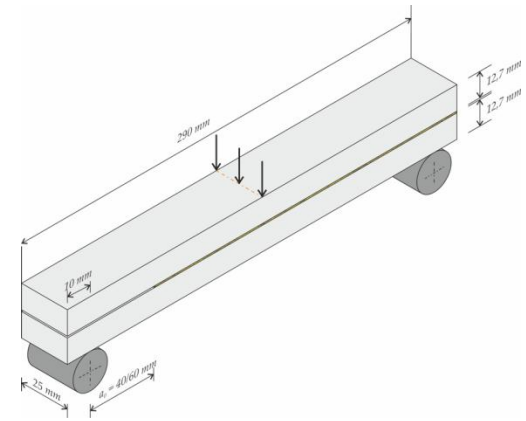

Figure 3. ENF specimen and test.

4ENF - 4 Points End Notch

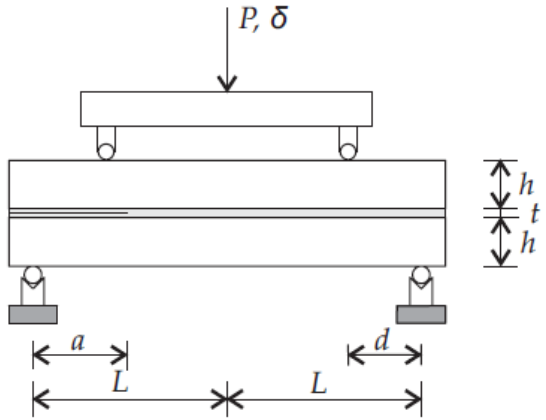

Figure 4. 4 ENF scheme

ELS – End Load Split

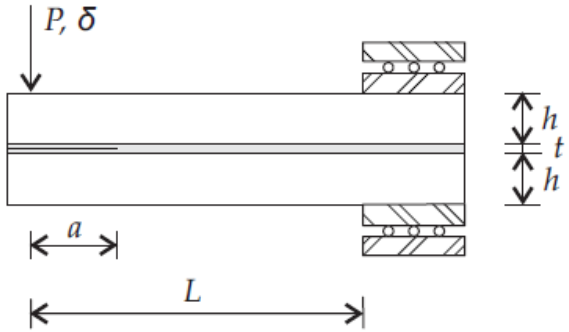

Figure 5. ELS scheme

fracture tests [mode II]

Mixed-Mode I + II release rates energies $G_T = G_{IC} + G_{IIC}$.

Crack Lap Shear [CLS]

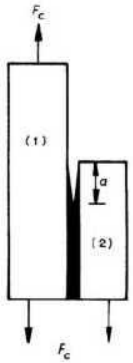

Edge Delamination Tension [EDT]

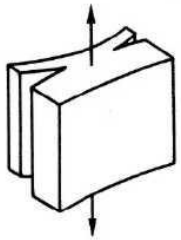

Arcan

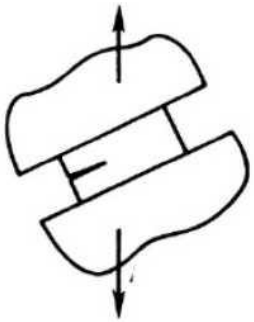

MMF – Mixed Mode Flexure (SLB)

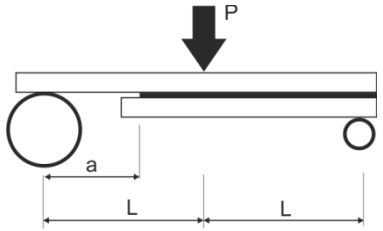

Mixed Mode Bending [MMB] **ASTM D6671**

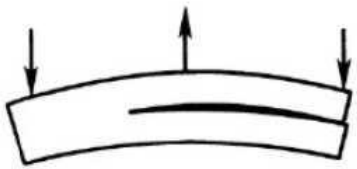

Asymmetrical Double Cantilever Beam [ADCB]

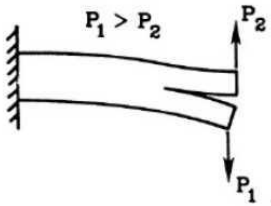

Asymmetrical Tapered Double Cantilever Beam [ATDCB]

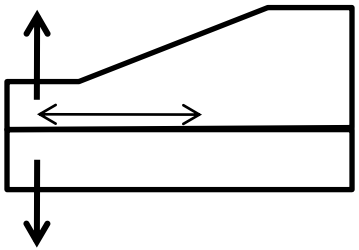

Dual Actuator Loading Frame [DAL]

SPELT JIG

Figure 6. Conventional test schemes for mixed-mode I + II.

fracture tests [mixed-mode I+II]

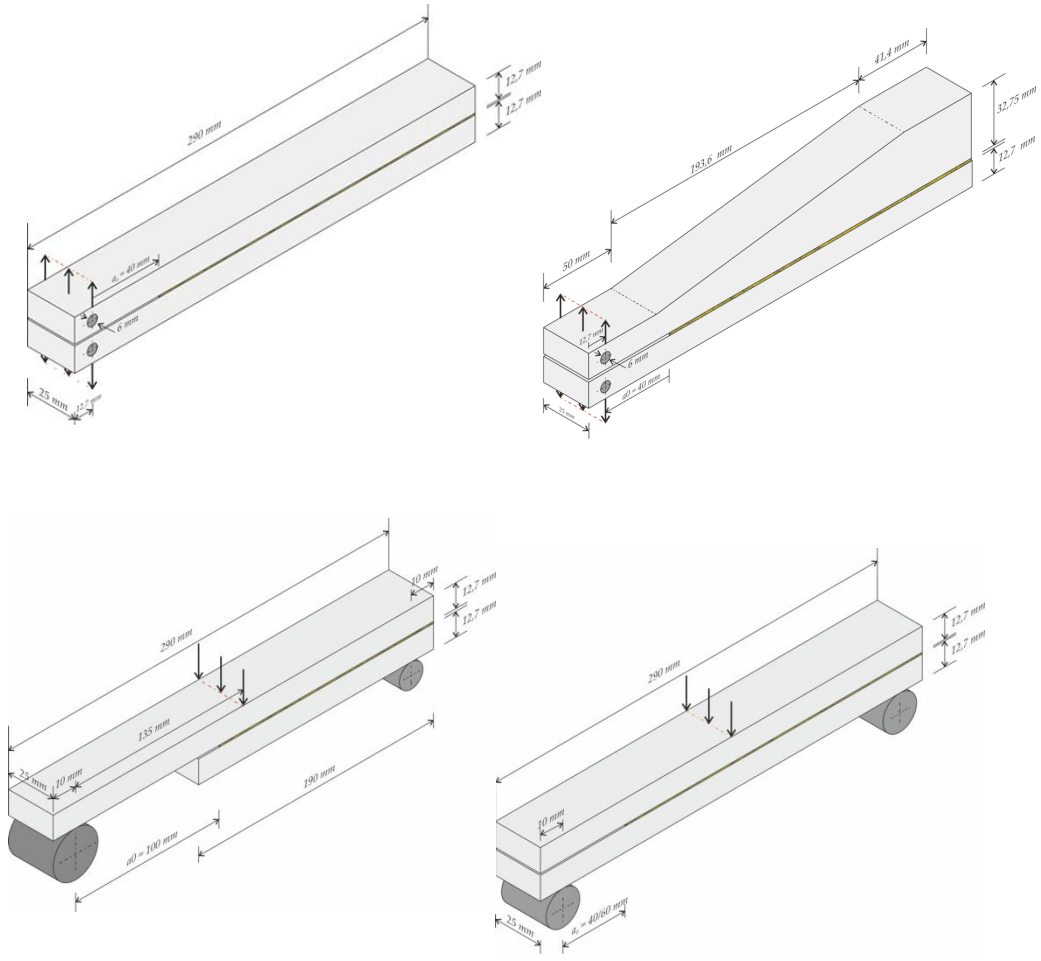

Figure 7. DCB, ATDCB, SLB and ENF specimen geometries.

Bondline thickness = 0.2 mm

Table1. Adhesive shear properties using the thick adherend shear test method ISO 11003-2

	2015
Shear modulus G (MPa)	487 ± 77
Shear yield strength τ_{ya} (MPa)	17.9 ± 1.80
Shear strength τ_r (MPa)	17.9 ± 1.80
Shear failure strain γ_f (%)	43.9 ± 3.40

Table2. Steel adherend properties

Steel	DIN 40CrMnNiMo7.
Young modulus, E [Gpa]	205
Yield strength, σ_y [MPa]	~900
Shear strength, σ_y [MPa]	~1000
Strain, ε_f [%]	~15

fracture tests

Table 3. Fracture toughness obtained with the conventional testing methods (average and standard deviation).

Test type	G_{Ic} (N/mm)	G_{IIc} (N/mm)
DCB+	0.44 ± 0.05	–
ENF	–	2.1 ± 0.21
SLB*	0.34 ± 0.06	0.32 ± 0.06
ADCB*	0.41 ± 0.04	0.004 ± 0.0005
ATDCB*	0.32 ± 0.04	0.07 ± 0.006

\+ Value corresponding to CBBM

* For these tests, the values indicated correspond to G_I and G_{II} and not G_{Ic} and G_{IIc}.

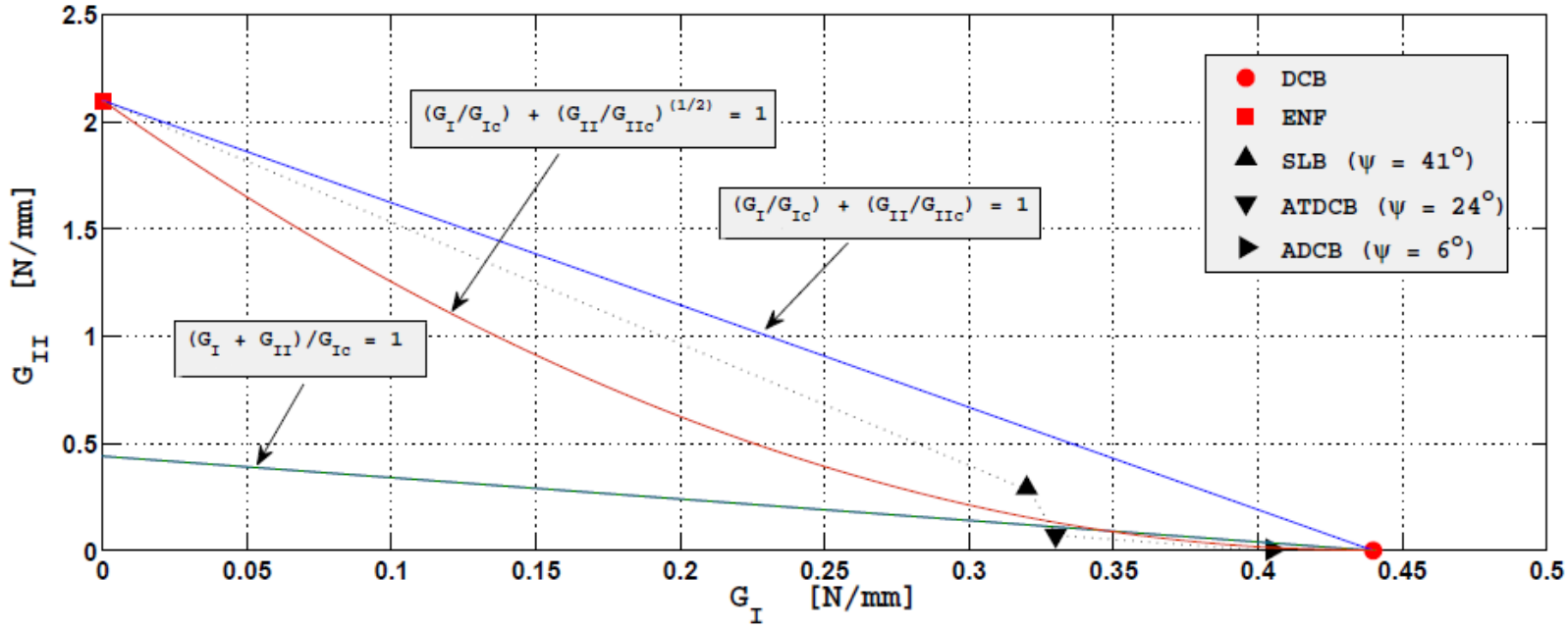

Figure 8. Fracture envelope for conventional tests.

fracture tests [envelope]

conventional – using the crack length measurement [a}

Compliance Calibration Method (CCM) is based on the Irwin-Kies theory (Trantina 1972, Kanninen and Popelar 1985)

Direct Beam Theory (DBT), based on elementary beam theory (Ding 1999)

Corrected Beam Theory (CBT) (Robinson and Das 2004, Wang and Williams 1992)

non-conventional – using the equivalent crack length [a_e]

The Compliance Based Beam Method (CBBM) was recently developed by de Moura et al. (2008, 2009) and is based on the crack equivalent concept

The Dual Actuator Load Frame (DAL) test is based on a DCB specimen loaded asymmetrically by means of two independent hydraulic actuators

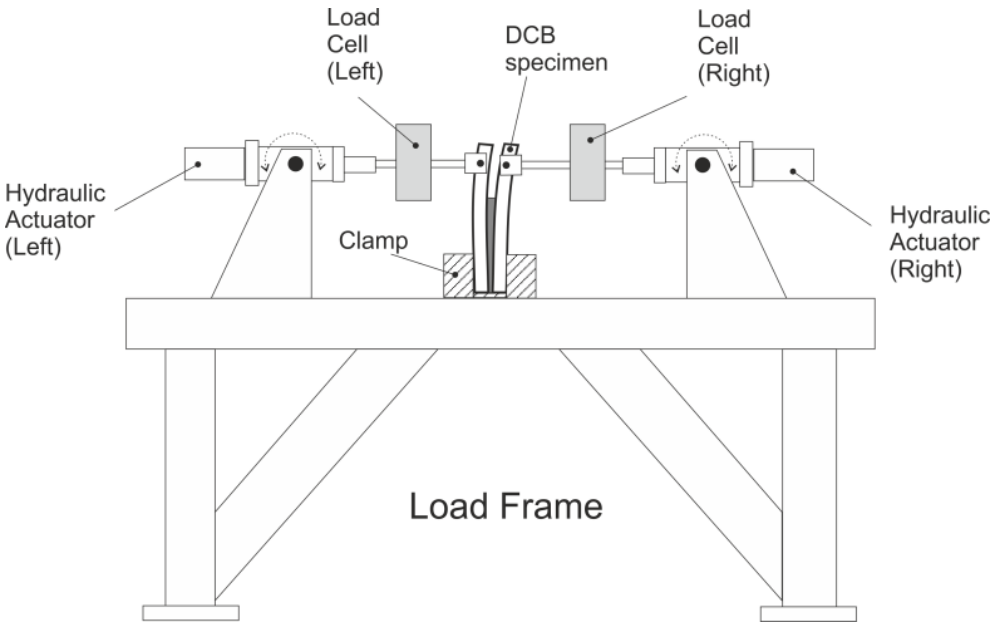

Figure 10. DAL frame

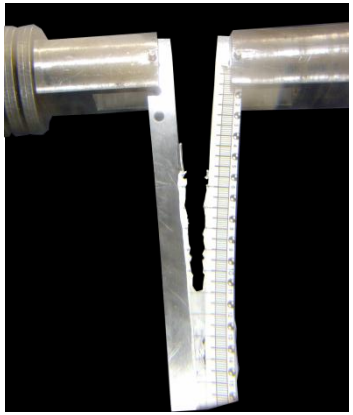

Figure 9. DAL loading a DCB specimen.

Different combinations of applied displacement rates provide different levels of mode ratios, thus allowing an easy definition of the fracture envelope in the G_I versus G_{II} space.

Dillard et al., 2009, J. Adhes. Sci. Technol. 23, 1515–1530

fracture tests [DAL]

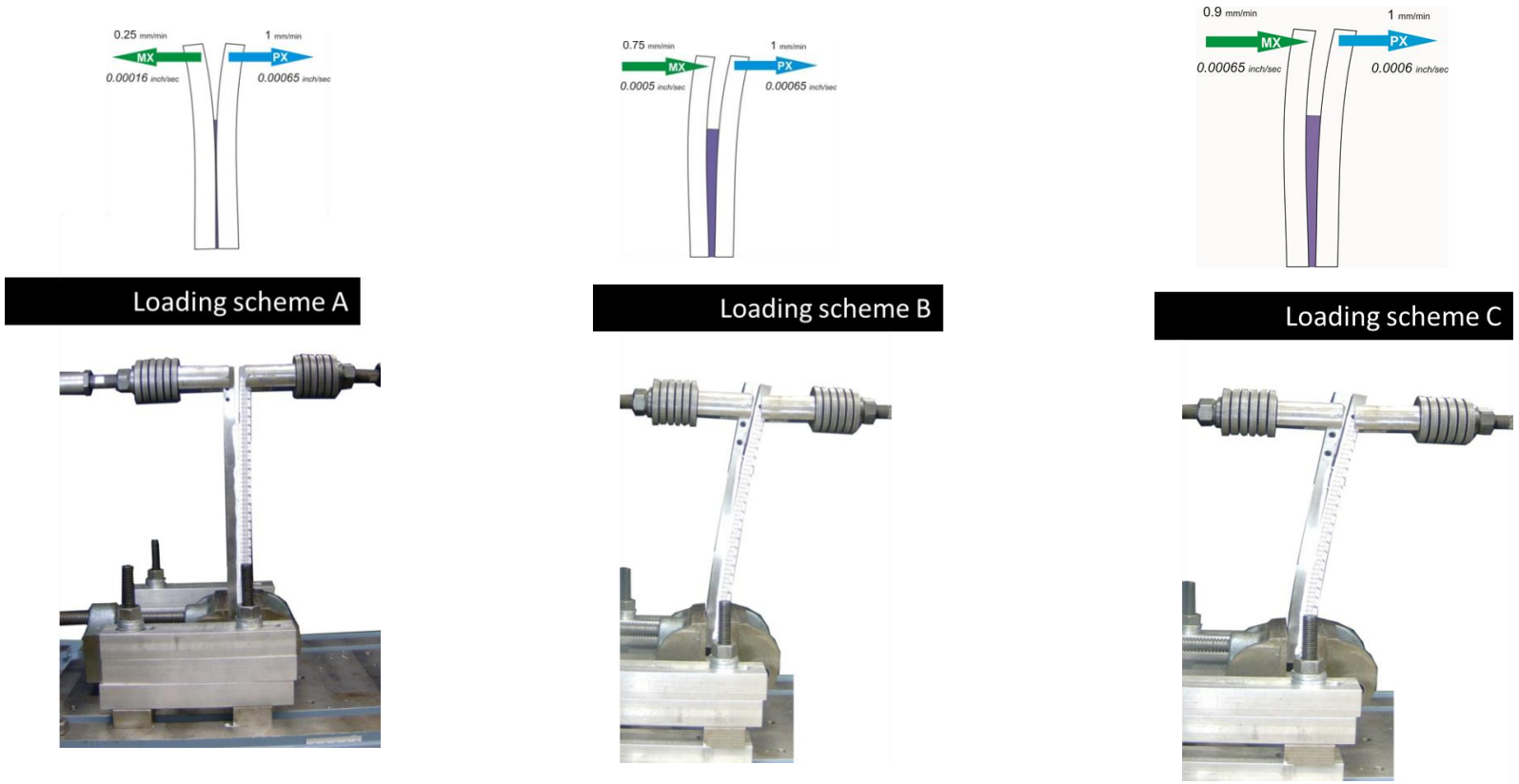

Figure 11. Loading schemes.

Classical data reduction schemes based on compliance calibration and beam theories require crack length monitoring during its growth, which in addition to FPZ ahead of the crack tip can be considered important limitations.

- non-conventional techniques [mixed-mode I+II]

Using Timoshenko beam theory, the strain energy of the specimen due to bending and including shear effects is:

$$U = \int_0^a \frac{M_R^2}{2EI_R}dx + \int_0^a \frac{M_L^2}{2EI_L}dx + \int_a^L \frac{M_T^2}{2EI}dx + \int_0^a \int_{-h/2}^{h/2} \frac{\tau_R^2}{2G} B\,dydx + \int_0^a \int_{-h/2}^{h/2} \frac{\tau_L^2}{2G} B\,dydx + \int_a^L \int_{-h}^{h} \frac{\tau_T^2}{2G} B\,dydx \quad (1)$$

M is the bending moment

subscripts R and L stand for right and left adherends

T refers to the total bonded beam (of thickness 2*h*)

E is the longitudinal modulus

G is the shear modulus

B is the specimen and bond width

I is the second moment of area of the indicated section

For adherends with same thickness, considered in this analysis, $I = 8I_R = 8I_L$

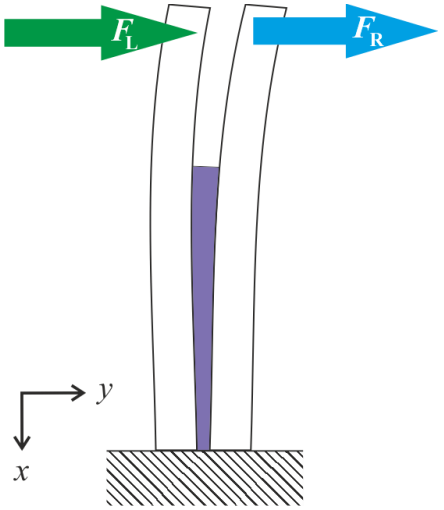

Figure 12. Schematic representation of loading in the DAL test.

non-conventional techniques [mixed-mode I+II]

The shear stresses induced by bending are given by:

$$\tau = \frac{3}{2}\frac{V}{Bh}\left(1-\frac{y^2}{c^2}\right) \qquad (2)$$

c - beam half-thickness

V - transverse load ⟶ on each arm for $0 \le x \le a$, and on total bonded beam for $a \le x \le L$

From Castigliano's theorem $\delta = \partial U / \partial P$

- P is the applied load
- δ is the resulting displacement at the same point

the displacements of the specimen arms can be written as

$$\delta_L = \frac{\left(7a^3+L^3\right)F_L}{2Bh^3E} + \frac{(L^3-a^3)F_R}{2Bh^3E} + \frac{3L\left[(F_L+F_R)+a(F_L-F_R)\right]}{5BhG}$$

$$\delta_R = \frac{\left(7a^3+L^3\right)F_R}{2Bh^3E} + \frac{(L^3-a^3)F_L}{2Bh^3E} + \frac{3L\left[(F_L+F_R)+a(F_R-F_L)\right]}{5BhG} \qquad (3)$$

non-conventional techniques [mixed-mode I+II]

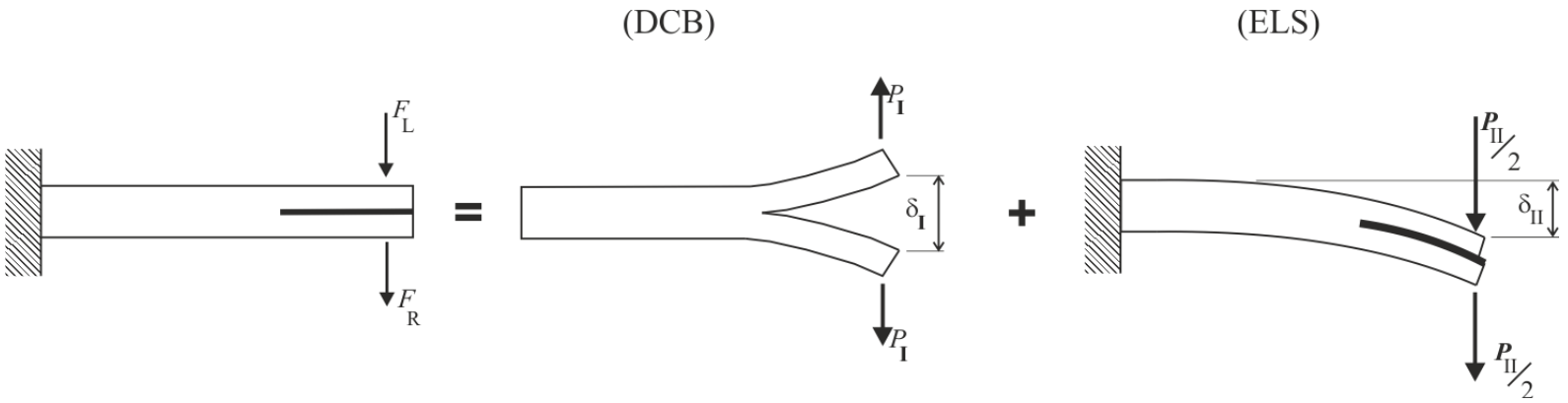

Figure 13. Schematic representation of loading in the DAL test.

pure mode loading

$$P_I = \frac{F_R - F_L}{2} \qquad P_{II} = F_R + F_L \tag{4}$$

pure mode displacements

$$\delta_I = \delta_R - \delta_L \qquad \delta_{II} = \frac{\delta_R + \delta_L}{2} \tag{5}$$

- non-conventional techniques [mixed-mode I+II]

Combining equations (3-5), the pure mode compliances become

(6) $$C_{\mathrm{I}} = \frac{\delta_{\mathrm{I}}}{P_I} = \frac{8a^3}{Bh^3E} + \frac{12a}{5BhG}$$ and $$C_{\mathrm{II}} = \frac{\delta_{\mathrm{II}}}{P_{\mathrm{II}}} = \frac{3a^3 + L^3}{2Bh^3E} + \frac{3L}{5BhG}$$ (7)

However, stress concentrations, root rotation effects, the presence of the adhesive, load frame flexibility, and the existence of a non-negligible fracture process zone ahead of crack tip during propagation are not included in these equations

To overcome these drawbacks, equivalent crack lengths can be calculated from the current compliances C_{I} and C_{II} (eq. 6 and 7)

$$\alpha a_{\mathrm{eI}}^3 + \beta a_{\mathrm{eI}} + \gamma = 0$$

$$a_{\mathrm{eI}} = \frac{1}{6\alpha} A - \frac{2\beta}{A} \quad (8)$$

$$a_{\mathrm{eII}} = \left[\left(C_{\mathrm{II}} - \frac{3L}{5BhG} \right) \frac{2Bh^3E}{3} - \frac{L^3}{3} \right]^{1/3} \quad (9)$$

$$\alpha = \frac{8}{Bh^3E}; \quad \beta = \frac{12}{5BhG}; \quad \gamma = -C_{\mathrm{I}}$$

$$A = \left(\left(-108\gamma + 12\sqrt{3\left(\frac{4\beta^3 + 27\gamma^2\alpha}{\alpha} \right)} \right) \alpha^2 \right)^{\frac{1}{3}}$$

non-conventional techniques [mixed-mode I+II]

The strain energy release rate components can be determined using the Irwin-Kies equation:

$$G = \frac{P^2}{2B}\frac{dC}{da} \quad (10)$$

combined with equation 6 →

$$C_{\mathrm{I}} = \frac{\delta_{\mathrm{I}}}{P_I} = \frac{8a^3}{Bh^3E} + \frac{12a}{5BhG}$$

$$G_{\mathrm{I}} = \frac{6P_{\mathrm{I}}^2}{B^2h}\left(\frac{2a_{\mathrm{eI}}^2}{h^2E} + \frac{1}{5G}\right) \quad (11)$$

combined with equation 7 →

$$C_{\mathrm{II}} = \frac{\delta_{\mathrm{II}}}{P_{\mathrm{II}}} = \frac{3a^3 + L^3}{2Bh^3E} + \frac{3L}{5BhG}$$

$$G_{\mathrm{II}} = \frac{9P_{\mathrm{II}}^2 a_{\mathrm{eII}}^2}{4B^2h^3E} \quad (12)$$

- The method only requires the data given in the load-displacement (P-δ) curves of the two specimen arms registered during the experimental test.
- Accounts for the Fracture Process Zone (FPZ) effects, since it is based on current specimen compliance which is influenced by the presence of the FPZ.

non-conventional techniques [mixed-mode I+II]

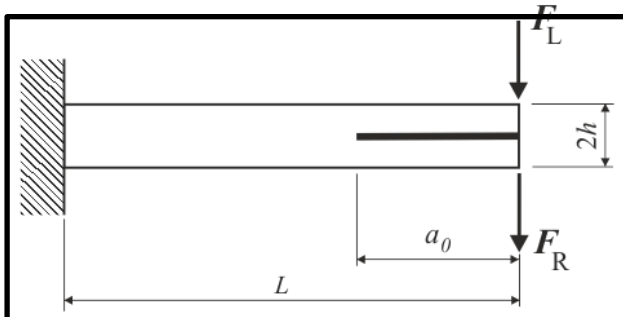

Figure 14. Specimen geometry used in the simulations of the DAL test

Numerical analysis including a cohesive damage model was carried out to verify the performance of the test and the adequacy of the proposed data reduction scheme.

Table 4. Elastic and cohesive properties.

Elastic properties (Steel)		Cohesive properties (Adhesive)			
E (GPa)	G (MPa)	$s_{u,I}$ (MPa)	$s_{u,II}$ (MPa)	G_{Ic} (N/mm)	**G_{IIc} (N/mm)**
210	**80.77**	**23**	**23**	**0.6**	**1.2**

The specimen was modelled with 7680 plane strain 8-node quadrilateral elements and 480 6-node interface elements with null thickness placed at the mid-plane of the bonded specimen.

non-conventional techniques [mixed-mode I+II]

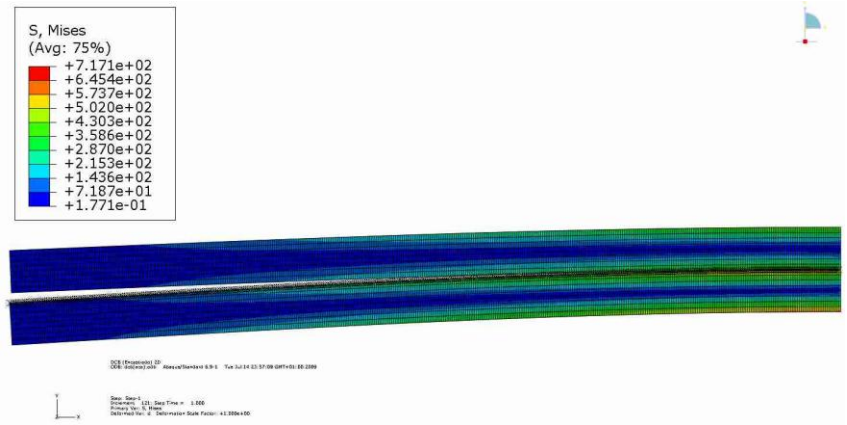

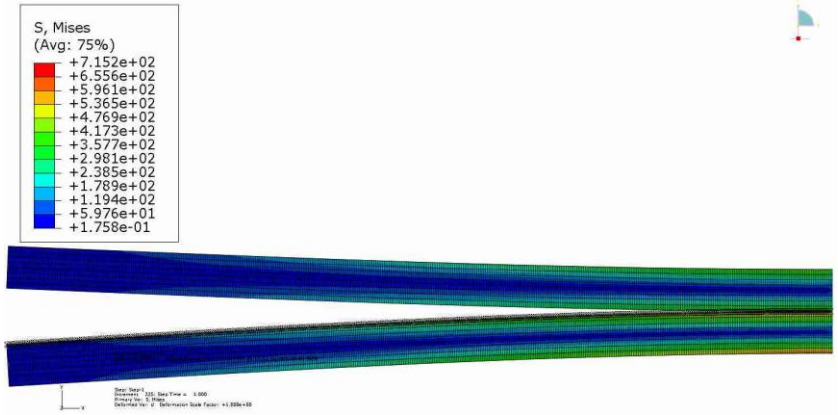

Figure 15. ABAQUS simulation mixed-mode (left) mode I (right)

a

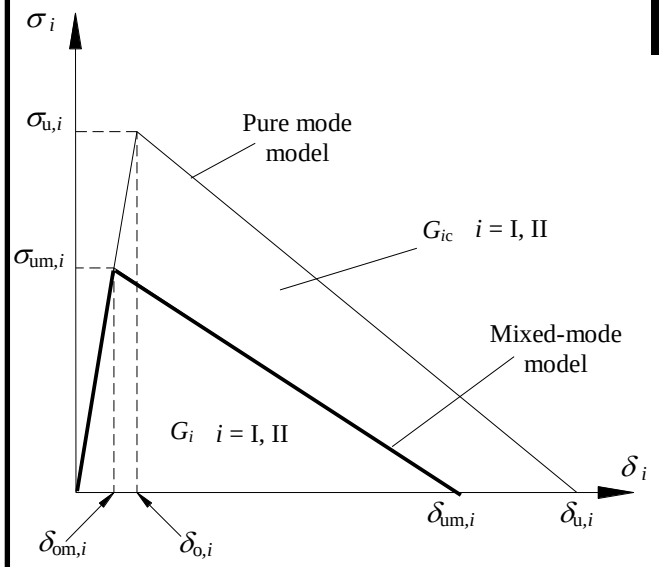

Figure 16. The linear softening law for pure and mixed-mode cohesive damage model.

b quadratic stress criterion to simulate damage initiation

$$\left(\frac{\sigma_{\mathrm{I}}}{\sigma_{\mathrm{u,I}}}\right)^2+\left(\frac{\sigma_{\mathrm{II}}}{\sigma_{\mathrm{u,II}}}\right)^2=1 \qquad (13)$$

c the linear energetic criterion to deal with damage growth

$$\left(\frac{G_{\mathrm{I}}}{G_{\mathrm{Ic}}}\right)+\left(\frac{G_{\mathrm{II}}}{G_{\mathrm{IIc}}}\right)=1 \qquad (14)$$

non-conventional techniques [mixed-mode I+II]

It is useful to define the displacement ratio

$$\lambda = \delta_L / \delta_R$$

- $\lambda = -1$ pure mode I
- $\lambda = 1$ pure mode II

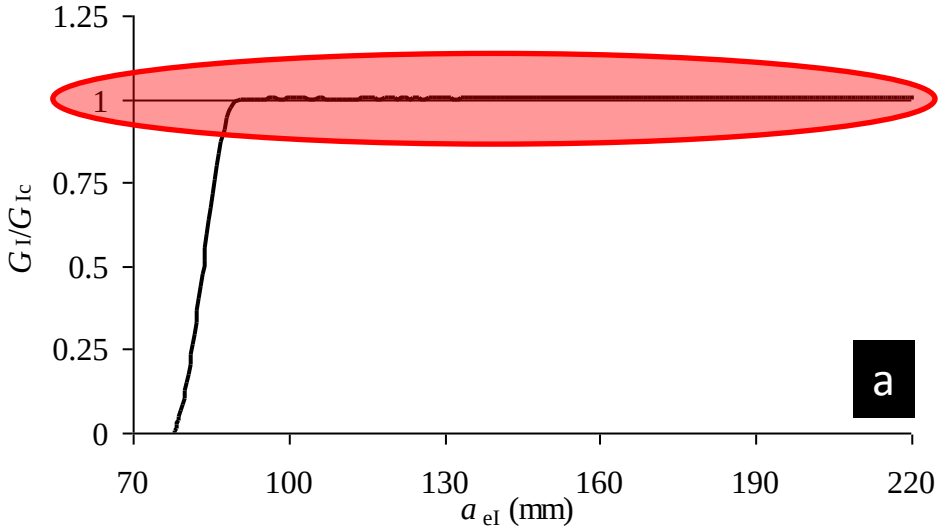

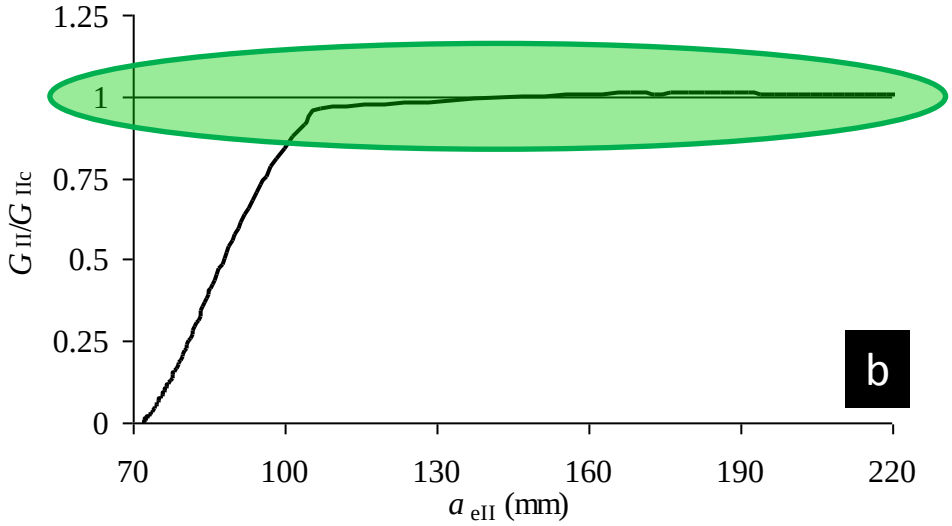

Figure 17. Normalized *R*-curves for the pure modes loading: a) Mode I; b) Mode II.

non-conventional techniques [mixed-mode I+II]

six different cases were considered in the range $-0.9 \leq \lambda \leq -0.1$

in this case mode I loading clearly predominate

nine combinations were analysed for $0.1 \leq \lambda \leq 0.9$

a large range of mode ratios is covered

Table 5. Imposed displacements for each simulation

	imposed displacem.	
Simul. #	beam 1	beam 2
1	10	-9
2	10	-8
3	10	-7
4	10	-5
5	10	-3
6	10	-1
7	10	0
8	10	1
9	10	3
10	10	5
11	10	7
12	10	7.5
13	10	8
14	10	8.5
15	10	9

non-conventional techniques [mixed-mode I+II]

variation of mode-mixity as the crack grows

for $\lambda = 0.7$, the *R*-curves vary as a function of crack length

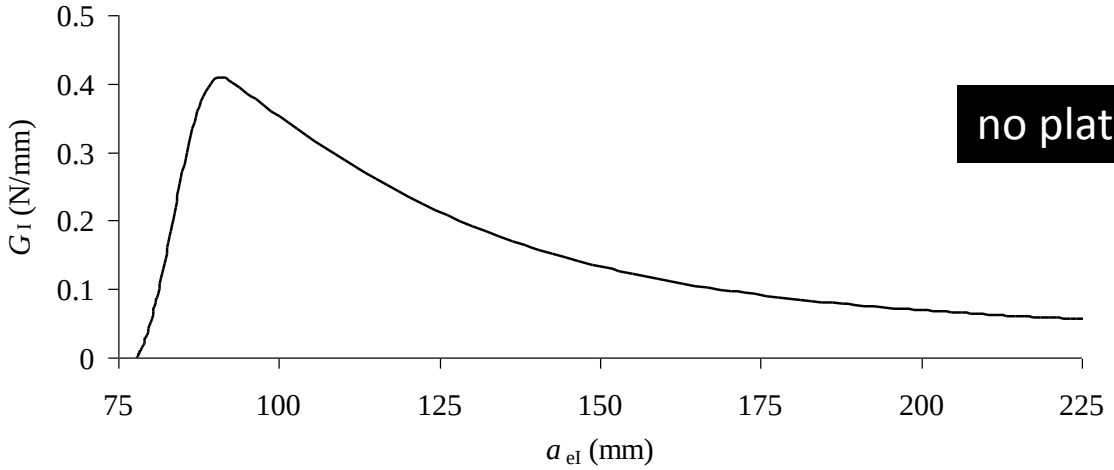

no plateau

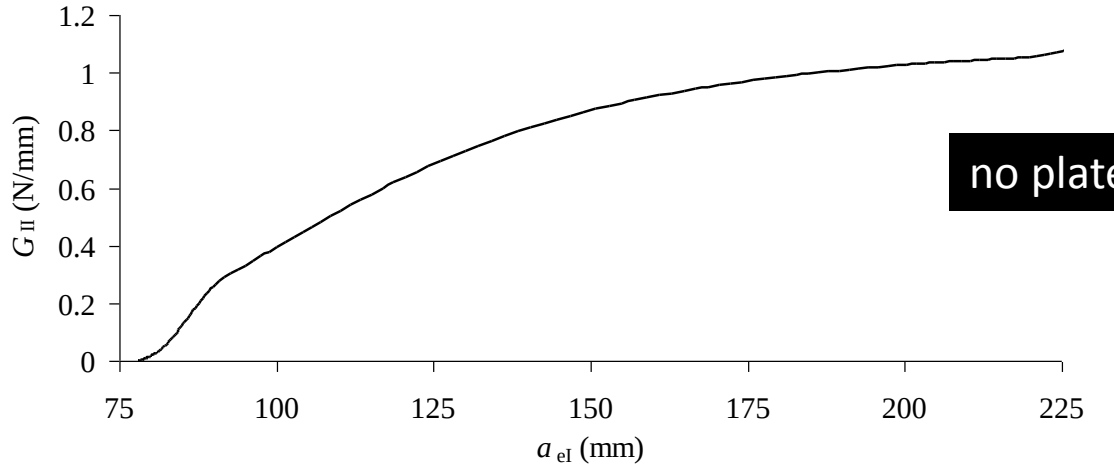

no plateau

Figure 18. *R*-curves for $\lambda = 0.7$ (both curves were plotted as function of a_{el} for better comparison).

non-conventional techniques [mixed-mode I+II]

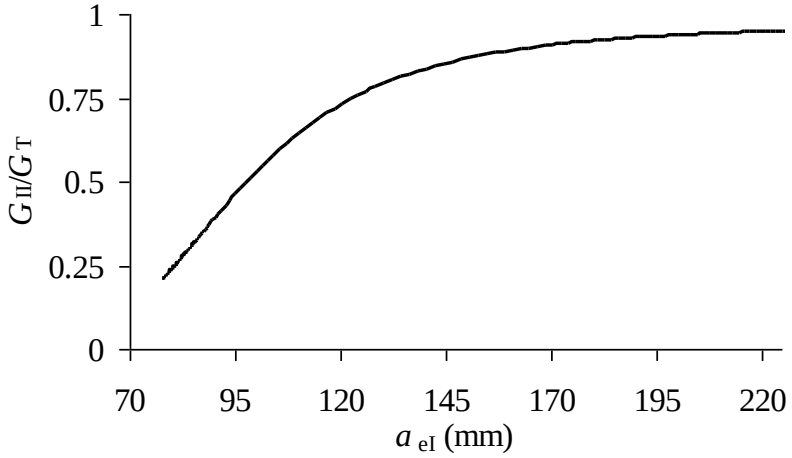

Figure 19. Evolution of mode mixity during propagation for $\lambda = 0.7$.

the proportion of mode II component increases as the crack propagates, being sensibly constant close to the end of the test

($G_T = G_I + G_{II}$)

FPZ length (l_{FPZ}) varies during crack growth as a consequence of the mode-mixity variation

l_{FPZ} is approximately constant near to the end of the test

is in agreement with the approximately constant mode-mixity observed in figure 19.

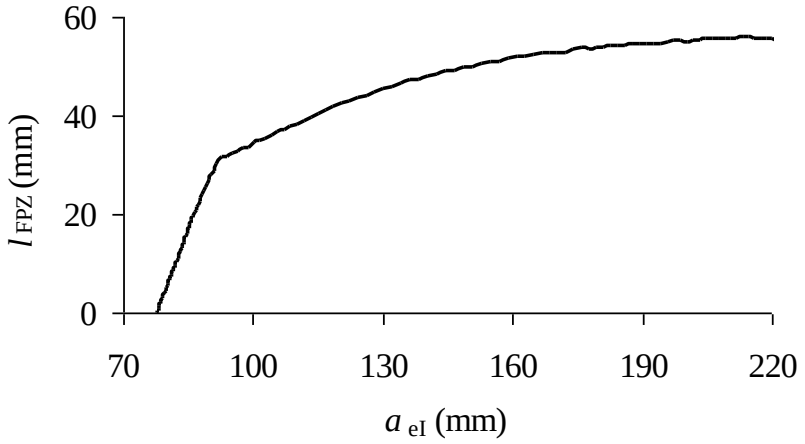

Figure20. FPZ length during crack growth.

non-conventional techniques [mixed-mode I+II]

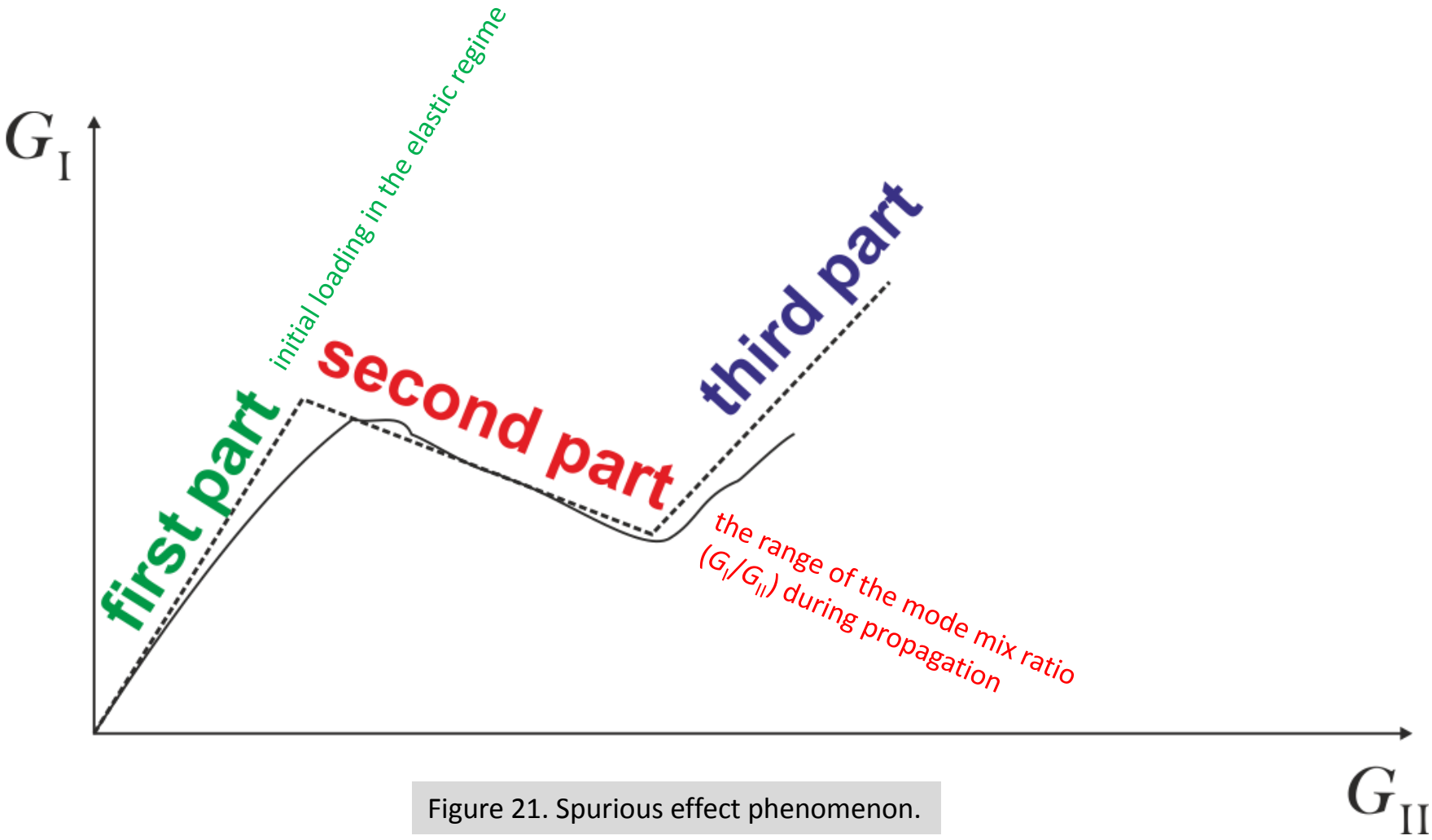

Figure 21. Spurious effect phenomenon.

the curves were cut at the beginning of the inflexion caused by the referred effects

non-conventional techniques [mixed-mode I+II]

mode I predominant loading conditions

combinations -0.9 ≤ λ ≤ -0.7, are nearly pure mode I loading conditions

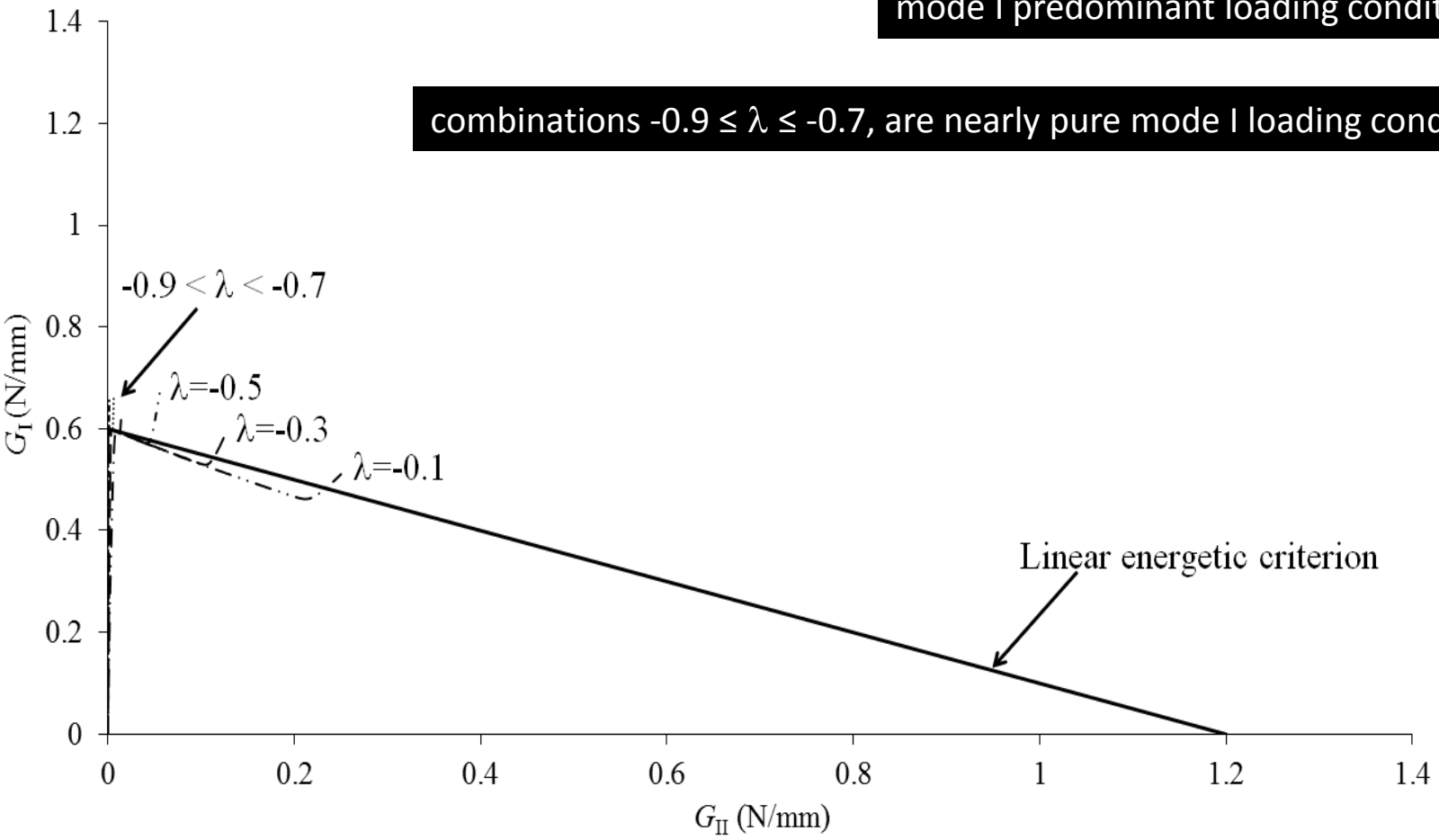

Figure 22. Plot of the G_I versus G_{II} strain energy components for -0.9 ≤ λ ≤ -0.1.

non-conventional techniques [mixed-mode I+II]

combinations using the positive values of λ induce quite a large range of mode ratios during crack propagation

excellent reproduction of the inputted linear criterion in the vicinity of pure modes, presenting a slight difference where mixed-mode loading prevail

explained by the non self-similar crack growth, which is more pronounced in these cases

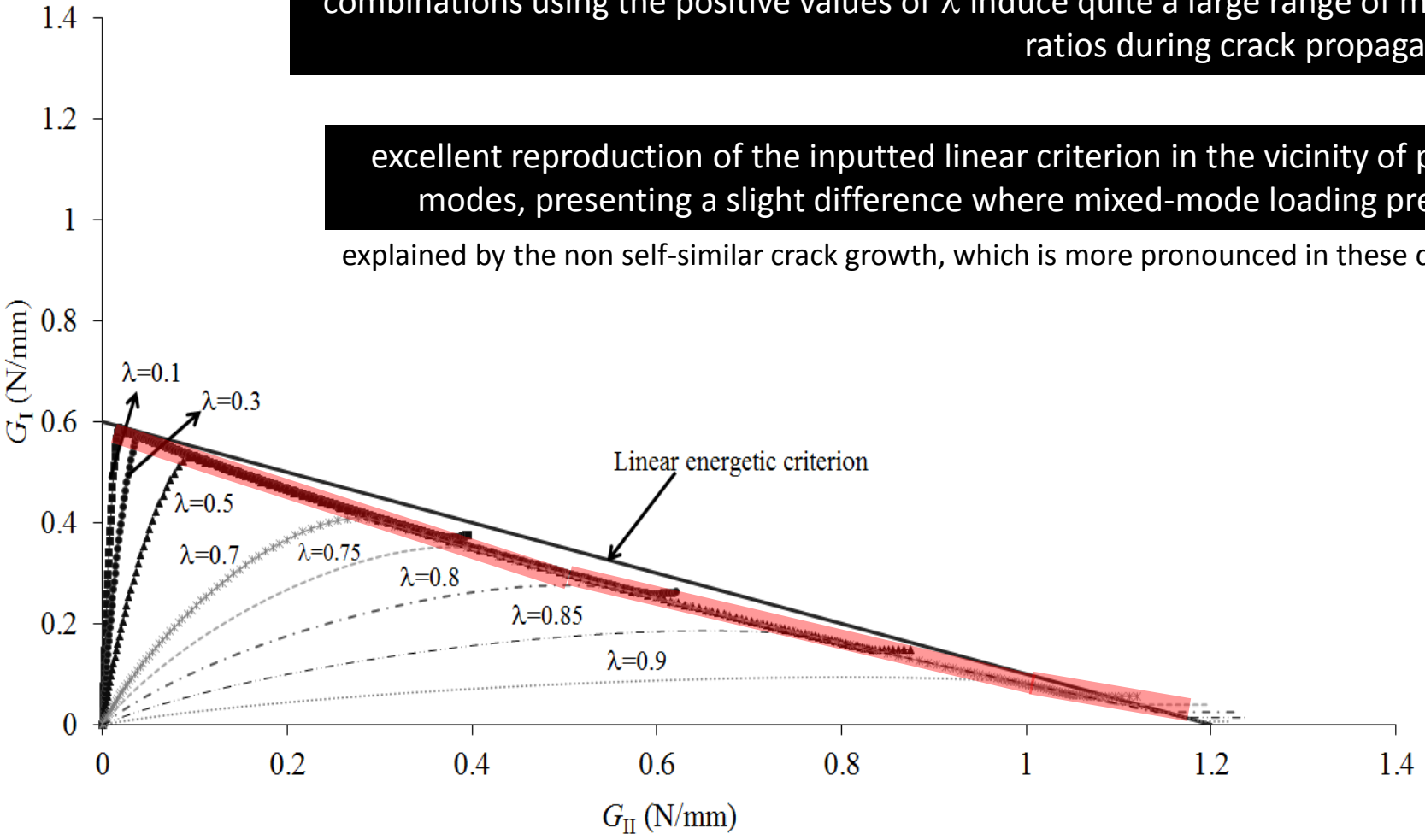

Figure 23. Plot of the G_I versus G_{II} strain energies for $0.1 \leq \lambda \leq 0.9$.

non-conventional techniques [mixed-mode I+II]

practically the entire fracture envelope can be obtained using only two combinations ($\lambda = 0.1$ and $\lambda = 0.75$) **important advantage of the DAL test**

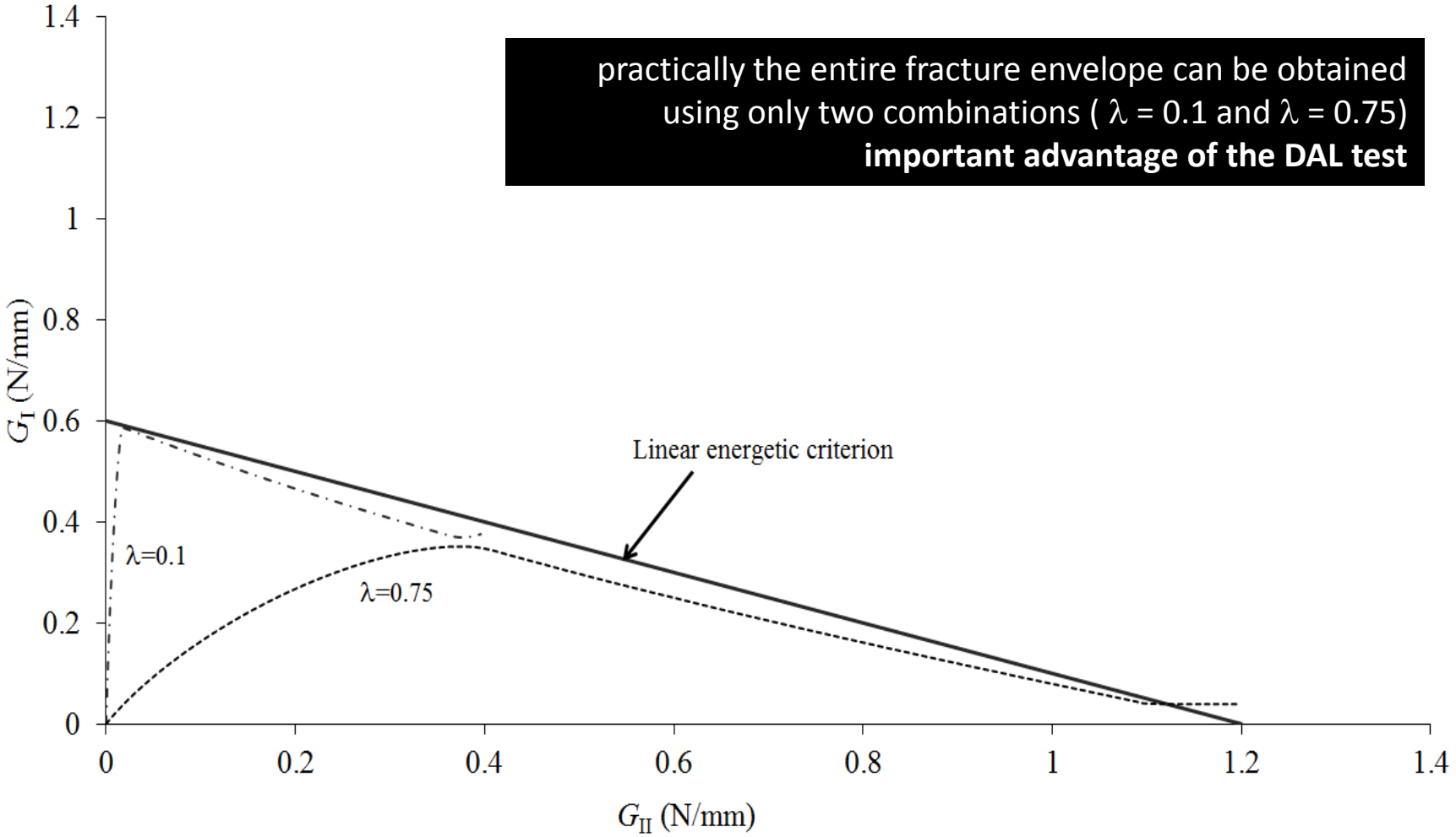

Figure 24. Plot of the G_I versus G_{II} strain energies for $\lambda = 0.1$ and $\lambda = 0.75$.

non-conventional techniques [mixed-mode I+II]

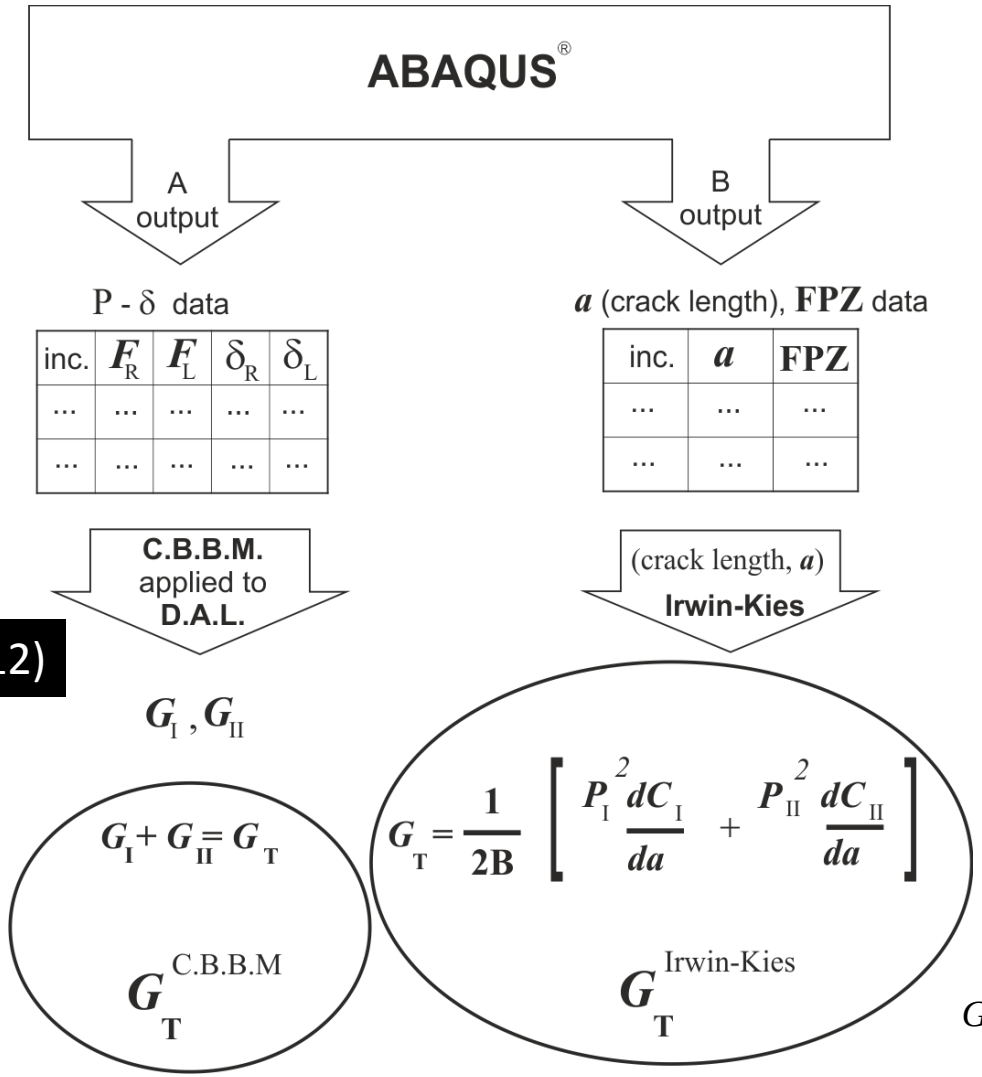

(11) & (12)

$$G_T = \frac{F_R^2}{2B}\frac{dC_R}{da} + \frac{F_L^2}{2B}\frac{dC_L}{da} \qquad (15)$$

- non-conventional techniques [mixed-mode I+II]

it can be concluded that both methods provide consistent results

agreement increases as the conditions of self-similar crack propagation (constant FPZ length – Figure 20) become more evident.

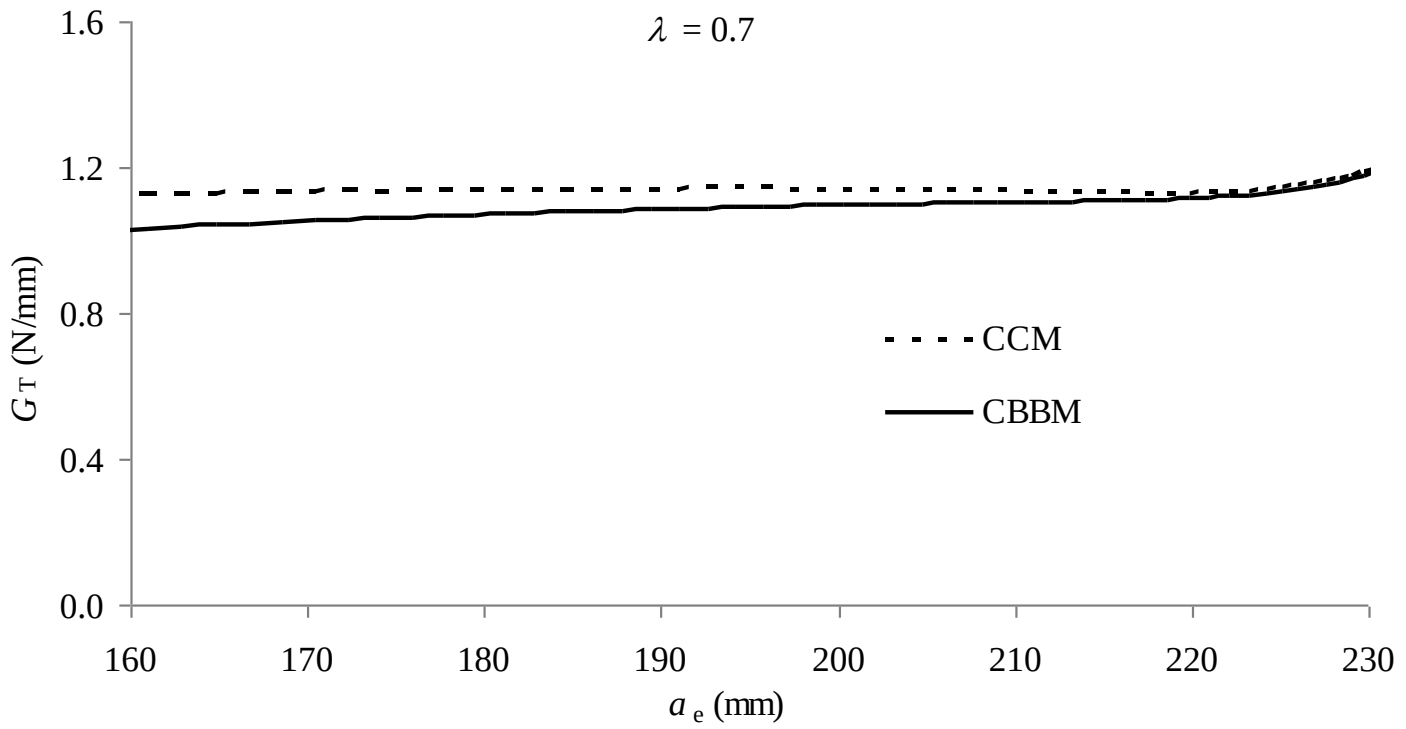

Figure 25. Plot of the G_T strain energy for $\lambda = 0.7$ obtained with CCM and CBBM.

non-conventional techniques [mixed-mode I+II]

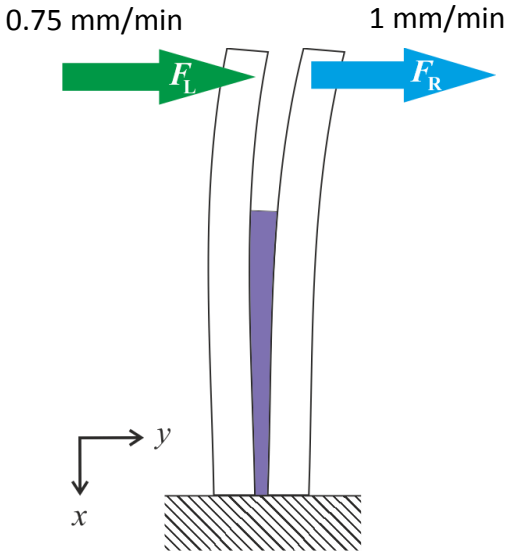

Figure 26. Schematic representation of loading scheme 2 with λ = 0.75 .

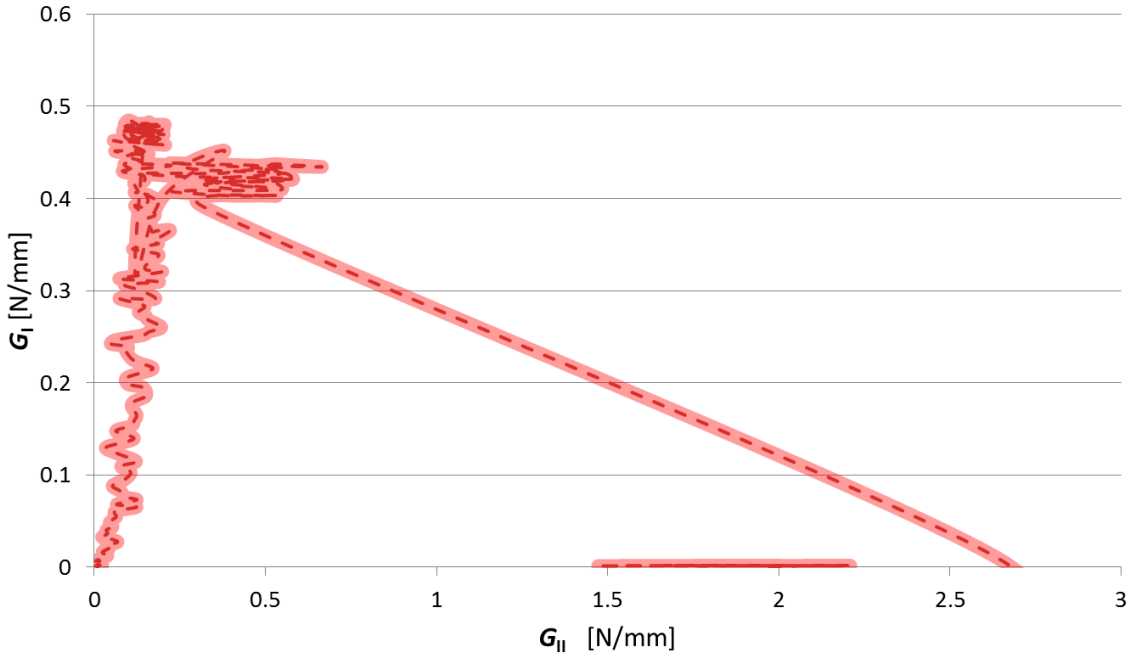

Figure 27. Envelope for Araldite 2015 with 0.2 mm bondline and λ = 0.75.

non-conventional techniques [mixed-mode I+II]

From table 3.

$$\begin{cases} G_I = 0.44 \pm 0.05 \text{ [N/mm]} \\ G_{II} = 2.1 \pm 0.21 \text{ [N/mm]} \end{cases}$$

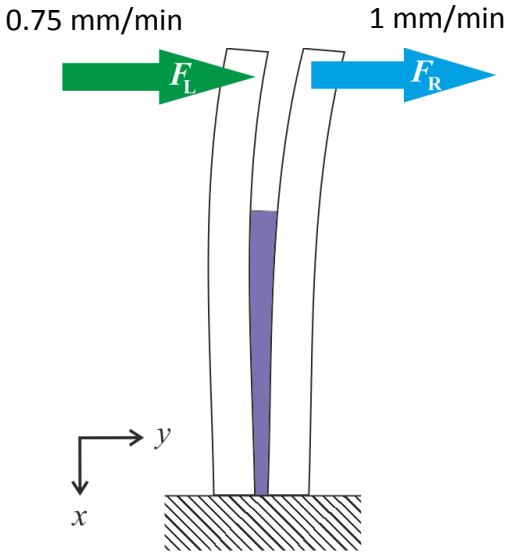

Figure 26. Schematic representation of loading scheme 2 with λ = 0.75 .

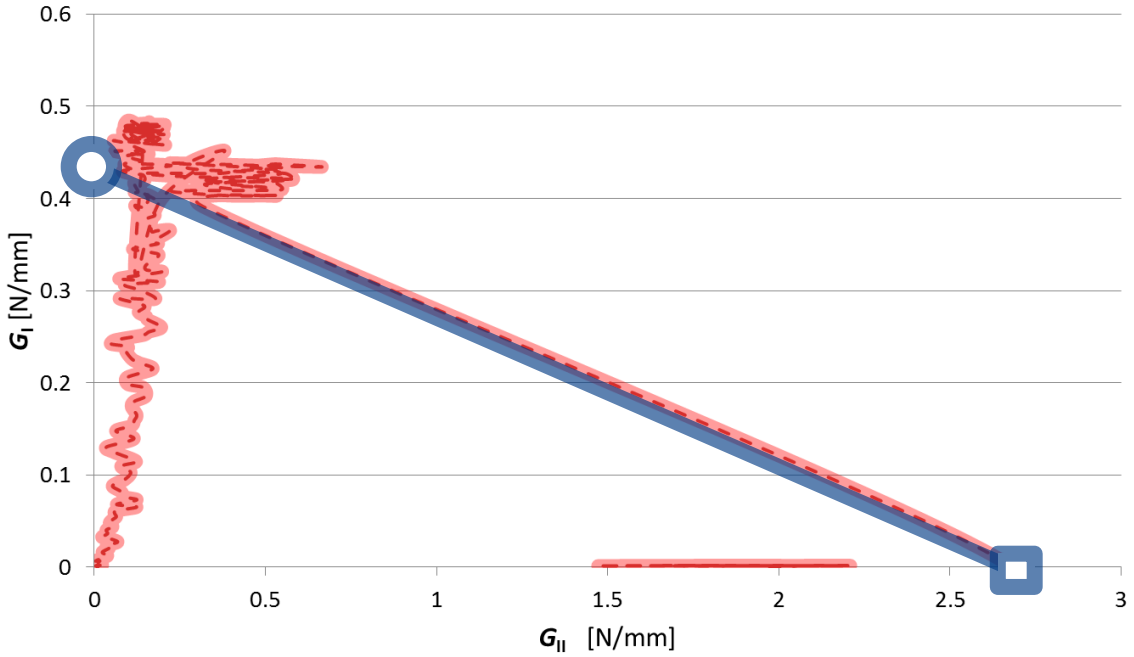

Figure 27. Envelope for Araldite 2015 with 0.2 mm bondline and λ = 0.75.

non-conventional techniques [mixed-mode I+II]

Mixed-mode testing is being implemented with a specimen load jig similar to the one that Spelt proposed, using DCB specimens used for the pure mode I (DCB) and pure mode II (ENF) and also for mixed-mode DAL.

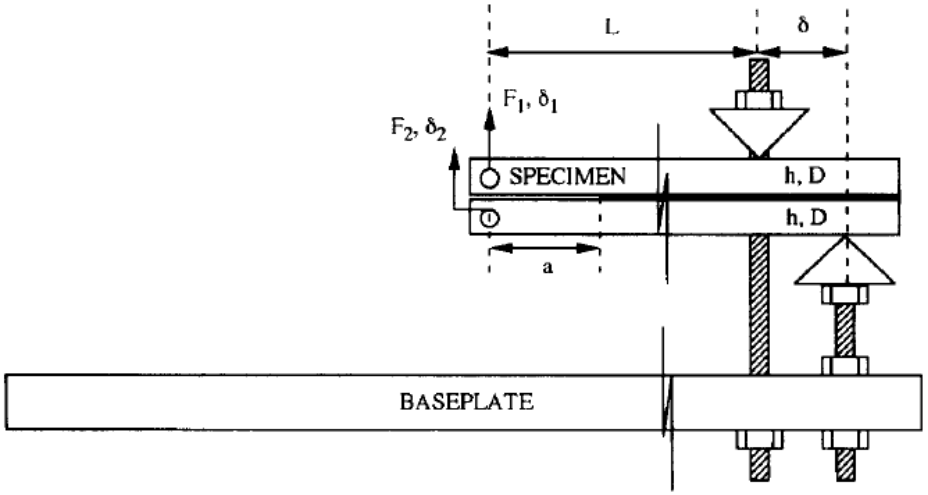

G. Fernlund & J. K. Spelt, *Composites Science and Technology* **50** (1994) 441-449

Figure 28. Load jig specimen geometry.

Figure 29. Specimen tested with the Spelt load jig.

non-conventional techniques [mixed-mode I+II]

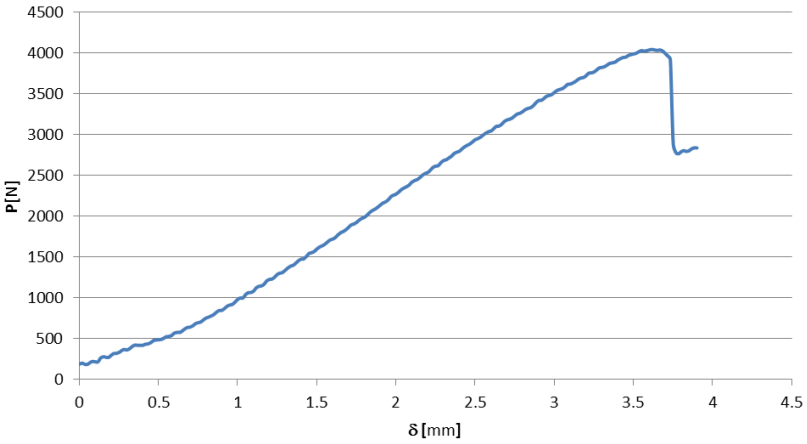

Figure 30. P-δ curve for Ψ = 56º

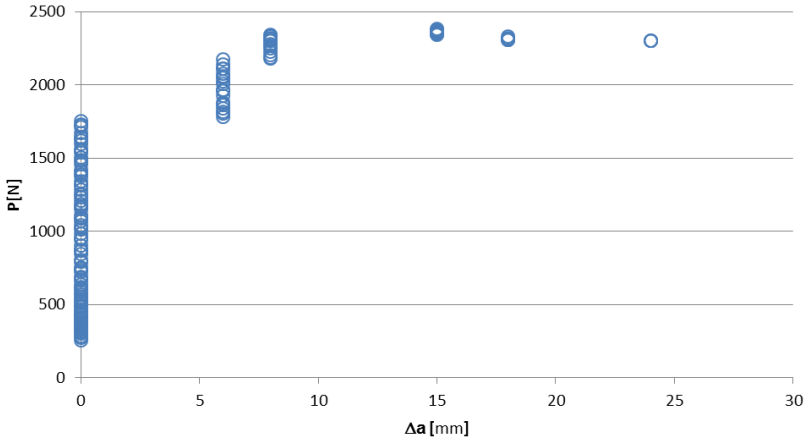

Figure31. P-Δa curve for Ψ = 56º

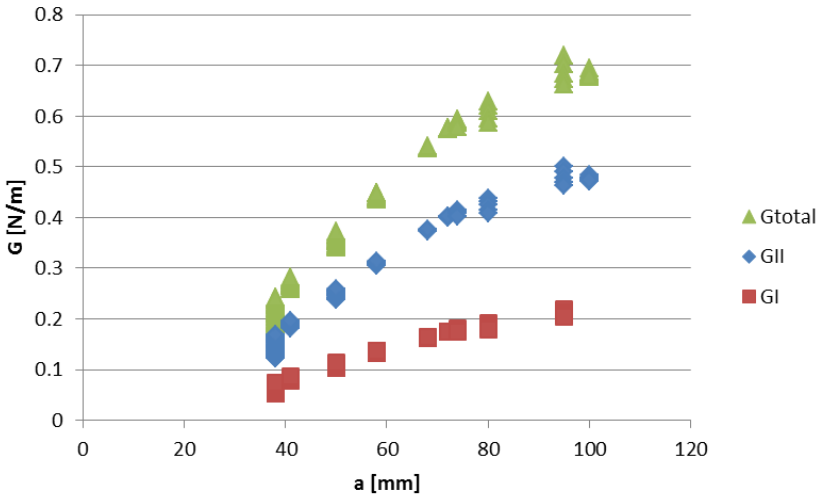

Figure 32. R curve for Ψ = 56º

- non-conventional techniques [mixed-mode I+II]

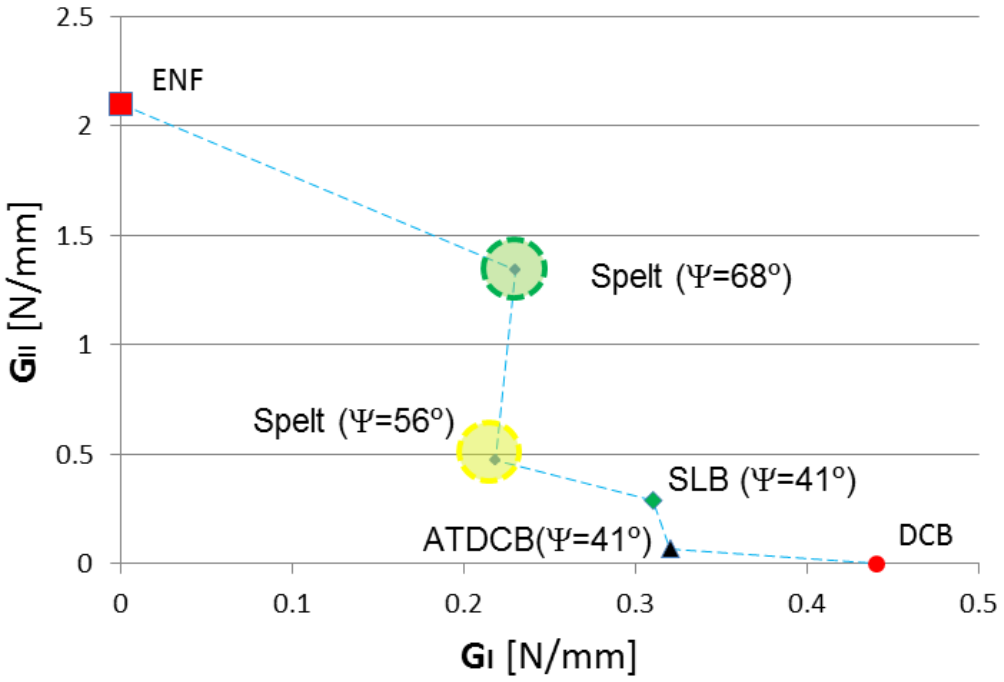

Figure 33. Preliminary envelope for $\Psi = 56^{o}$

non-conventional techniques [mixed-mode I+II]

The specimen was modelled with 3992 plane strain 8-node quadrilateral elements and 382 6-node interface elements with null thickness placed at the mid-plane of the bonded specimen.

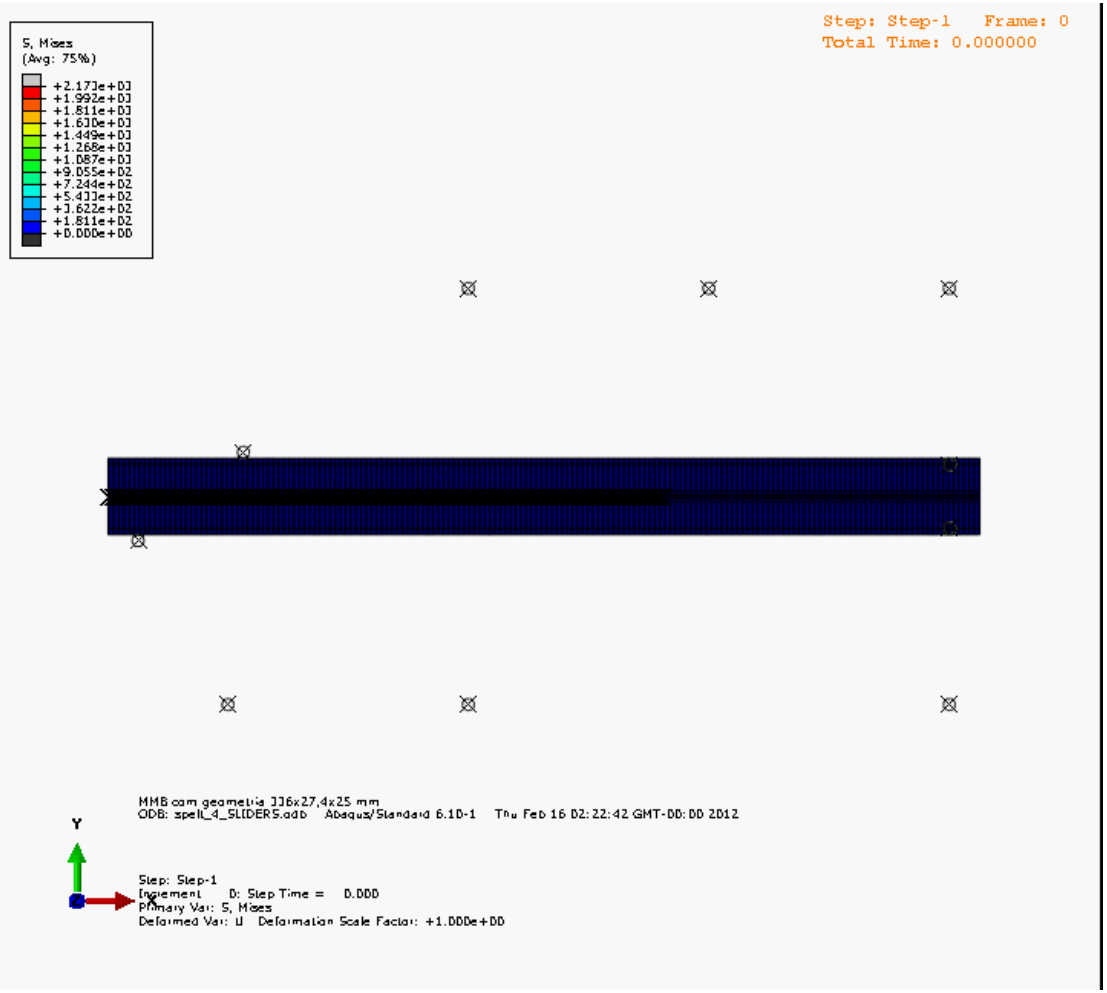

The goal is to develop a CBBM for the Spelt Specimen load jig .

Obtain the envelope for different bondline thicknesses, with this jig and the analytical tool (CBBM) .

non-conventional techniques [mixed-mode I+II]

conclusions

- a new data reduction scheme based on specimen compliance, beam theory and crack equivalent concept was proposed to overcome some problems intrinsic to the DAL test
- the model provides a simple mode partitioning method and does not require crack length monitoring during the test, which can lead to incorrect estimation of fracture energy due to measurements errors
- since the current compliance is used to estimate the equivalent crack length, the method is able to account indirectly for the presence of a non-negligible fracture process zone (very important for ductile adhesives)
- for pure modes I and II, excellent agreement was achieved with the fracture values inputted in the cohesive model
- in some cases the mixed-mode ratio alters significantly during crack propagation, thus leading to non self-similar crack growth
- the positive values of the displacement ratio (λ) covered almost all the fracture envelope
- a slight difference relative to the inputted linear energetic criterion was observed in the central region of the G_I versus G_{II} plot, corresponding to mixed-mode loading, which is attributed to the non self-similar crack propagation conditions that are more pronounced in these cases
- only two combinations of the displacement ratio are sufficient to cover almost all the adhesive fracture envelope

Develop a CBBM data reduction scheme for the Spelt specimen load jig .

Obtain the envelope for different bondline thicknesses, with this jig and the analytical tool (CBBM) .

future work

The authors would like to thank the contribution of Edoardo Nicoli, and Youliang Guan for their work in experimental testing at Virginia Tech.

The authors also acknowledge the financial support of Fundação Luso Americana para o Desenvolvimento (FLAD) through project 314/06, 2007 , IDMEC and FEUP.

Thank you.

Thank you.